Raman and infrared spectroscopy of pyridine under high pressure

Kirill K. Zhuravlev, Katrina Traikov, Zhaohui Dong, Shuntai Xie, and Yang Song*
Department of Chemistry, University of Western Ontario, London, Ontario, Canada N6A 5B7

Zhenxian Liu
Geophysical Laboratory, Carnegie Institution of Washington, 5251 Broad Branch Road NW, Washington, DC 20015, USA

(Received 3 May 2010; revised manuscript received 30 June 2010; published 30 August 2010)

We report the structural transitions of pyridine as a function of pressure up to 26 GPa using *in situ* Raman spectroscopy and infrared absorption spectroscopy. By monitoring changes in the Raman shifts in the lattice region as well as the band profiles in both Raman and IR spectra, a liquid-to-solid transition at 1 GPa followed by solid-to-solid transitions at 2, 8, 11, and 16 GPa were observed upon compression. These transitions were found to be reversible upon decompression from 22 GPa. A further chemical transformation was observed when compressed beyond 22 GPa as evidenced by the substantial and irreversible changes in the Raman and infrared spectra, which could be attributed to the destruction of the ring structure. The observed transformations in pyridine were also compared to those for benzene. The similar transition sequence with well-aligned transition pressures suggests that these isoelectronic aromatics may have similar structures and stabilities under high pressure.

DOI: 10.1103/PhysRevB.82.064116 PACS number(s): 62.50.−p, 82.80.−d, 64.60.−i

I. INTRODUCTION

Aromatic compounds under nonambient conditions have been the subject of extensive research over the past few decades due to their great importance in both fundamental and applied science.[1] These compounds have been widely studied in chemical synthesis under elevated temperatures and pressures as the precursors of technological materials, such as conjugated polymers and amorphous solids.[2–8] In addition, rich structural, chemical, and phase behaviors have been observed in a broad pressure-temperature regions where new optical and thermodynamic properties have been characterized.[9–16] For instance, application of high pressure to benzene resulted in several structural changes and the formation of new compounds, such as crystalline and amorphous graphite materials, depending on the extreme conditions rendered.[2,8] When combined with compression, photon excitation of benzene significantly alters its high-pressure reaction pathway leading to the ring opening via unusual mechanisms.[5] Benzene derivatives in the form of conjugated polyphenyls, such as p-quaterphenyl and biphenyl that exhibited a twisted conformation at the ambient pressure, can be flattened upon the application of high pressure, causing the change in their optical properties.[13,14] Other aromatic compounds, such as thiophene and furane, were also found to exhibit intriguing pressure-induced structural transformations.[3,6,7]

Pyridine (C_5H_5N), a heterocyclic aromatic compound, resembles the well-known benzene structure (C_6H_6) by replacing one of the CH groups with a nitrogen atom. Isoelectronic to benzene, the structures and properties of pyridine have been extensively investigated by various experimental approaches at ambient pressure, including Raman spectroscopy,[17–20] infrared (IR) spectroscopy[17,18,21–24] as well as x-ray diffraction.[25] However, high-pressure studies of pyridine have been scarce.[26,27] Heyns and Venter reported that pyridine crystallizes at 1 GPa with another possible modification into a glassy phase.[26] It was found that the crystalline form of pyridine undergoes a phase transition at about 2 GPa. Based on the pressure dependence of Raman spectra and the number of lattice modes observed, it was concluded that pyridine at high pressure has a structure that is different from that obtained at low temperatures.[26] Solid pyridine at low temperature and ambient pressure has been determined to have an orthorhombic structure $Pna2_1(C_{2v}^9)$ with $Z=16$.[25] It was suggested that pyridine at high pressures crystallizes into a monoclinic structure, analogous to the benzene phase II structure with a space group $P2_1/m$,[28] although no structural analysis was available for pyridine. Other than these studies, the structures and stabilities of pyridine are completely unknown above 6 GPa, in strong contrast to benzene, whose phase diagram has been well established in a much broader region up to 50 GPa and 1000 K.[8]

In the present work, we report the results of Raman and IR spectroscopies on pyridine under pressures up to 26 GPa. We identified three additional reversible solid-to-solid phase transitions and one irreversible transition above a threshold compression pressure. Analyses of pressure dependence of Raman shifts as well as the Raman and IR profiles of pyridine allowed for the understanding of possible structural modifications of pyridine in parallel with those observed for benzene under high pressure.

II. EXPERIMENTAL

Pyridine (99.8%) was purchased from Sigma Aldrich as a clear liquid and was loaded in a diamond anvil cell (DAC) without further purification. DACs were equipped with a pair of type I or type II diamonds (both with a culet size of 400 μm) for respective Raman and IR measurements. Ruby chips were placed in the sample chamber to serve as *in situ* pressure gauge. The pressure was determined by measuring the optical shift of ruby R_1 fluorescence line.[29] No other pressure transmitting medium was used. No significant line broadening was detected in the entire pressure region, indi-

cating nearly hydrostatic conditions inside the pressure chamber. Pressure increments were 0.5–1.5 GPa upon compression and 2–3 GPa upon decompression, respectively. Raman spectra were obtained using a custom-made microspectroscopy system. Ar^+ laser line of 514.5 nm was used as the excitation source and was focused onto the DAC by an optical microscope with a laser beam size of a few microns on the sample. The scattered light was collected in a backscattering geometry and analyzed by an Acton spectrometer equipped with an 1800 lines/mm grating providing a resolution better than 1 cm^{-1} and a liquid-nitrogen-cooled charge coupled device detector. The system was calibrated using neon lines with an uncertainty of ± 1 cm^{-1}. A pair of notch filters was used to block the Rayleigh line thus enabling a measurable spectral range above 100 cm^{-1}. All measurements were taken at room temperature.

Infrared spectroscopy was performed at the U2A beamline at the National Synchrotron Light Source (NSLS), Brookhaven National Laboratory (BNL). The IR beam from the storage ring was extracted through a wedged diamond window from a source at a 40×40 $mrad^2$ solid angle and was collimated to a 1.5 in. diameter beam before entering a Bruker IFS 66V vacuum Fourier transform infrared (FTIR) spectrometer in conjunction with three microscope systems. For mid-IR measurements, the IR beam was focused on the sample using a Bruker IR microscope and then the spectrum was collected in transmission mode by a mercury cadmium telluride detector in the 600–8000 cm^{-1} spectral range. A resolution of 4 cm^{-1} was used in all IR measurements. For IR measurements, a sample thickness of 35 μm was used to allow sufficient IR transmission. For all measurements, mid-IR spectra were collected through a 30×30 μm^2 aperture. The reference spectrum, i.e., the diamond anvil absorption at ambient pressure was later divided as background from each sample spectrum to obtain the absorbance.

III. RESULTS AND DISCUSSION

A. Raman and IR spectra at ambient pressure

The Raman and IR spectra of pyridine collected at near ambient conditions (i.e., at 0.2–0.6 GPa) are depicted in Fig. 1 as the starting point for subsequent compression. The C_{2v} point-group symmetry for pyridine molecule implies that among the 27 possible vibrational modes, all are Raman active (i.e., A_1, A_2, B_1, and B_2 modes) while 24 modes are IR active (i.e., A_1, B_1, and B_2 modes). In our measurements, 13 Raman- and 17 IR-active modes were identified. The list of all the observed modes along with their frequencies and assignments is given in Table I. We followed the assignment proposed by Urena *et al.*[30] and labeled the modes accordingly in Fig. 1. As can be seen, our results are in close agreement with those obtained for liquid pyridine in previous studies.[18,20,26]

B. Raman spectra upon compression

We collected Raman spectra of pyridine upon compression with selected spectra shown in Figs. 2 and 3 in the lattice modes region and internal modes region, respectively.

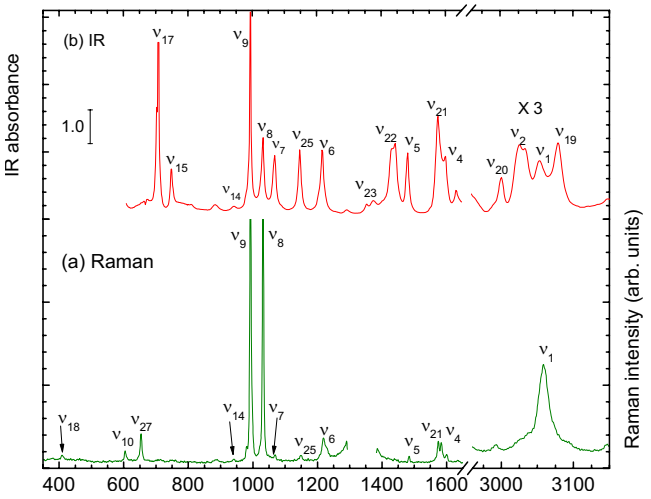

FIG. 1. (Color online) Raman spectrum of pyridine (a) in comparison with the IR spectrum (b) in the internal mode region of 375–3250 cm^{-1}, both collected at near-ambient pressure. The left vertical axis denotes IR absorbance (with the absolute intensity labeled by the vertical bar) while the right axis refers to Raman intensity. The IR spectrum in the region of 2950–3200 cm^{-1} has been scaled by a factor of 3. The region from 1300 to 1400 cm^{-1} was truncated due to the strong diamond T_{2g} mode in this region while the region of 1650–2950 cm^{-1} was omitted due to the lack of spectroscopic features of interest. The assignments are labeled for most fundamental vibrational modes. The unlabeled bands in the IR spectrum are overtones or combinations. See text and Table I.

When compressed to >1 GPa, a change in the physical appearance of the sample was observed under a microscope, indicating a liquid-to-solid transition, consistent with Heyns's observation.[26] Upon further compression, we observed a total of five Raman modes in the lattice region (labeled from 1 to 5 from low to high frequencies). Due to the cutoff of the notch filter, modes below 80 cm^{-1}, if any, cannot be resolved unambiguously. At about 2 GPa, two lattice modes at 130 and 166 cm^{-1} (labeled as 4 and 5) emerged, suggesting a solid-to-solid transition. Further compression to 8.1 GPa resulted in the appearance of another prominent lattice mode at 90 cm^{-1} (labeled as 1). Additional lattice modes at 222 and 204 cm^{-1} (labeled as 3 and 2) were observed upon subsequent compression to 11.3 GPa and 15.5 GPa, respectively. Each of the occurrences of a new lattice mode suggests a possible phase transition.

In the internal mode region of 400–1100 cm^{-1} [Fig. 3(a)], the Raman patterns show no prominent changes upon compression. However, a marked increase in intensity together with a splitting was observed for the ring stretch and CH bend mode ν_6 at 1241 cm^{-1} when compressed to 2.4 GPa [Fig. 3(b)]. The splitting of this mode became most prominent at 8.1 GPa. Concurrently, the CH stretch mode ν_1 around 3084 cm^{-1} became a triplet. At 11.3 GPa, the two ring stretch and CH bend modes, ν_6 and ν_5, were significantly depleted together with further splitting and broadening of the ν_1 mode. Above 16.1 GPa, all modes exhibited significant broadening and weakening, leaving only two bands, ν_{21} and ν_1, observable in the spectral region above 1100 cm^{-1}. Finally, all internal modes were drastically de-

TABLE I. Assignment and frequencies (cm^{-1}) of observed Raman and IR internal modes of pyridine in comparison with reference values.

			Raman					Infrared	
Mode[a]	Symmetry[a]	Description[a]	This work[b]	This work[c]	Liquid[d]	Phase I[d]	Phase II[d]	This work[e]	Liquid[d]
ν_{18}	B_1	Out-of-plane ring bend	409	414	407	417	421		406
ν_{10}	A_1	In-plane ring bend	604	605	604	609	609		603
ν_{27}	B_2	In-plane ring bend	653	655	653	653	655		654
ν_{17}	B_1	CH wagging and ring out-of-plane bend						703	701
ν_{15}	B_1	CH wagging and ring out-of-plane bend			750			762	747
ν_{14}	B_1	CH wagging	941		942	1010	1016	941	941
ν_9	A_1	In-plane ring bend	993	999	991	998	1004	995	991
ν_8	A_1	In-plane ring bend	1031	1038	1031	1038	1041	1034	1030
ν_7	A_1	Ring stretch and CH bend	1069	1076	1069	1068	1067	1070	1069
ν_{25}	B_2	Ring stretch and CH bend	1149	1151	1147	1150	1150	1147	1146
ν_6	A_1	Ring stretch and CH bend	1218	1230	1217	1233	1237	1217	1217
ν_{23}	B_2	Ring stretch and CH bend			1355			1356	1355
ν_{22}	B_2	Ring stretch			1438			1444	1437
ν_5	A_1	Ring stretch and CH bend	1484	1489	1483			1483	1483
ν_{21}	B_2	Ring stretch and CH bend	1574	1579	1574	1577	1581	1577	1574
ν_4	A_1	Ring stretch and CH bend	1584	1589	1582	1588	1591	1600	1581
ν_1	A_1	CH stretch	3058	3084	3057	3070	3079	3053	3053

[a]Reference 30.
[b]Measured at 0.6 GPa.
[c]Measured at 2.5 GPa.
[d]Reference 26.
[e]Measured at 0.2 GPa.

pleted above 18.9 GPa and at 26 GPa, no Raman bands were observed (not shown).

C. Pressure dependence of lattice modes

The observed evolutions of the Raman profile in both the lattice and internal mode regions clearly and consistently suggest pressure-induced phase transitions. The transition boundaries as well as the transition mechanism may be better understood by examining the pressure dependences ($d\nu/dP$) of the characteristic vibrational modes. The pressure dependence of the Raman shifts of the lattice modes of pyridine is presented in Fig. 4 and Table II. The rates of Raman shifts were determined by linear regressions. As can be seen, the frequencies of all lattice modes blueshifted with increasing pressure, but with different rates in different regions. These changes in shift rates unambiguously outlined the pressure regions where new phases (labeled as II, III, IV, and V in addition to phase I, a pressure-condensed solid phase from liquid) were formed. Furthermore, the Raman-shift rate of all lattice modes exhibits a decreasing trend with pressure, indicating smaller compressibility for pyridine in higher pressure regions as a result of a denser molecular packing upon compression.

D. IR spectra upon compression

Supplementary to Raman measurements, we collected mid-IR spectra for pyridine upon compression in a similar pressure range. Selected IR spectra are depicted in Fig. 5. Starting as a liquid, pyridine was found to solidify when compressed to around 1 GPa as indicated by visual observation under a microscope. Compression from 1.5 to 2.4 GPa resulted in marked enhancement of IR intensity for modes ν_{14}, ν_{25}, and ν_{23} and the appearance of several new IR bands which are most likely combinations and/or overtones of fundamentals. In addition, splitting was observed for several IR modes, such as ν_9, ν_7, and ν_{22} with ν_6 being the most prominent which split into a triplet. At pressures above 8.1 GPa, the ν_{15} (748 cm^{-1}) and ν_5 (1485 cm^{-1}) modes became broadened and started to split whereas ν_6 (1217 cm^{-1}) mode evolved from a triplet to a doublet. The most dramatic change at this pressure is the switch of the relative intensity of the doublet components for ν_{17} and ν_{22} modes. Above 12 GPa, however, the previously split ν_{17} and ν_{22} modes each merged into a single band from a doublet. Moreover, when compressed to 16.7 GPa, the band intensity was significantly reduced for the ν_{17} mode while band broadening and merging (e.g., ν_{17} with ν_{15} modes and ν_{22} with ν_5 modes) were the common features observed in the IR spectra upon subsequent compression. Finally, some IR modes were completely depleted upon compression to pressures higher than 22 GPa (not shown), similar to the observation in the Raman measurements at pressures around 26 GPa. All these observed changes in the IR spectra shown in Fig. 5 are generally consistent with the phase transitions suggested by the corresponding Raman measurements.

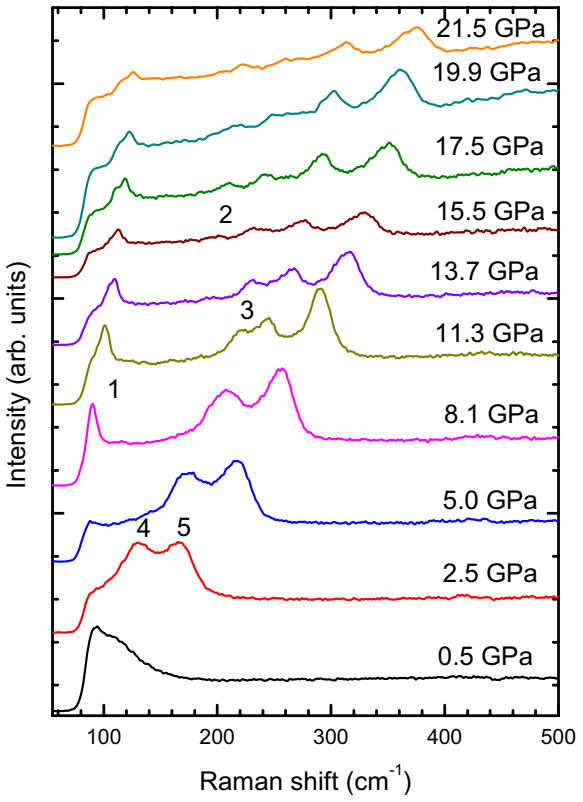

FIG. 2. (Color online) Selected Raman spectra of pyridine in the lattice mode region collected upon compression. The spectra are offset vertically for clarity. The pressures are labeled above each spectrum. The numbers 1–5 labels the five lattice modes observed during compression. See text.

E. Decompression

We performed two sets of compression-decompression cycles on pyridine by achieving different maximum pressures. In the first set, pyridine was compressed to ~22 GPa and then decompressed to near ambient pressure while in the second set the maximum pressure reached was around 26 GPa. Figure 6 shows the Raman spectra of pyridine upon decompression from ~22 GPa as the maximum pressure to a pressure of ~4 GPa in comparison with that recovered from 26 GPa as the maximum compression pressure. It is apparent that the pressure-induced transformations are almost completely reversible when the maximum compression pressure is less than 22 GPa while compression beyond that pressure resulted in an irreversible transformation as shown by the top spectrum in Fig. 6. Similar results were also obtained in the IR measurements. For instance, the IR spectra collected on decompression from a maximum compression pressure of 20 GPa to 0.4 GPa showed a complete reversibility for almost all spectral changes as shown in Figs. 7(a) and 7(b). In contrast, decompression from a maximum pressure above 22 GPa (e.g., 26.1 GPa) in another run resulted in dramatic and irreversible changes in the IR spectra as shown in Figs. 7(c) and 7(d). Sample recovered from 26.1 GPa exhibited a few weak bands (e.g., at 700 and 1450 cm^{-1}) and two broad bands around 1600 and 2900 cm^{-1} in the IR spectrum [Fig. 7(d)]. These peaks are likely associated with hydrocarbon stretches that involve carbon atoms with mixed hybridizations. The implications of these observations are discussed in the next section.

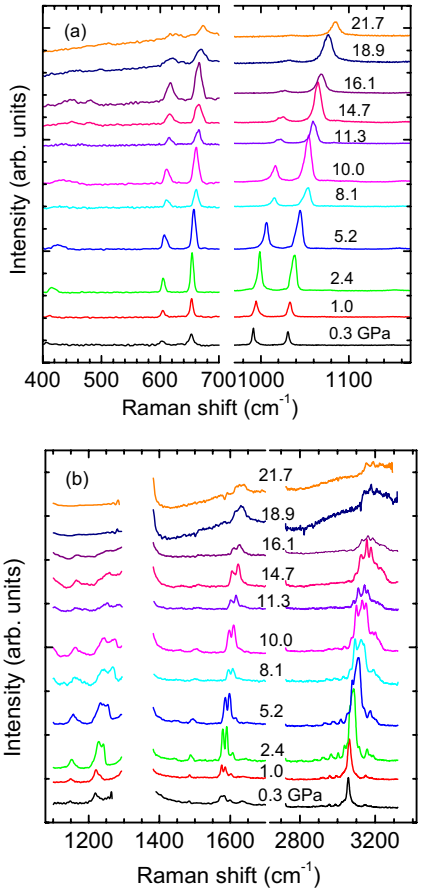

FIG. 3. (Color online) Raman spectra of pyridine on compression in the spectral region of (a) 400–1160 cm^{-1} and (b) 1100–3300 cm^{-1} at selected pressures. The ranges of 700–950 cm^{-1} and 1700–2800 cm^{-1} were omitted due to the lack of fundamental vibrational modes while the spectra were truncated in the region of 1300–1400 cm^{-1} due to the strong diamond T_{2g} mode in this region. The spectra are offset vertically for clarity.

F. Discussion

Our extensive Raman and IR measurements of pyridine on compression collectively and consistently suggest the existence of several distinct phases with boundaries at around 1, 2, 8, 11, and 16 GPa. While the transition at 1 GPa can be characterized as a liquid-to-solid transition, the subsequent transitions are solid-solid transitions associated with changes in crystal lattices and/or molecular structures. The only previous high-pressure study (up to 6 GPa) by Heyns and Venter indicated only one solid-to-solid phase transition at 2 GPa.[26] Based on the observation of several broad lattice modes at the transition pressure, they suggested the formation of a "glassy" state of pyridine. Although the number of lattice modes as well as the band profile in the lattice region observed in our Raman measurements are slightly different from those of Heyns's, the signature vibrational frequencies of all internal Raman modes observed at 2.5 GPa are in good

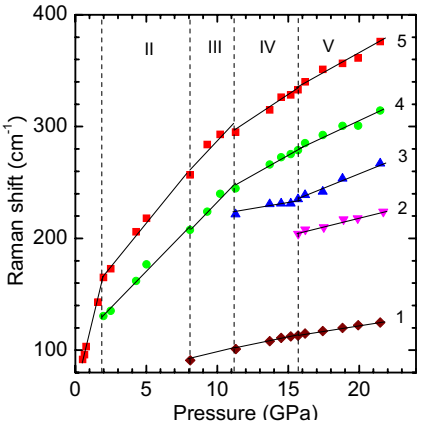

FIG. 4. (Color online) Raman shift of pyridine as a function of pressure on compression in the lattice mode region. Solid straight lines are linear fits to the data. Vertical dashed lines mark the suggested phase transition boundaries. Different symbols denote lattice modes with different origins with numbers labeled from low to high frequencies. See text and Fig. 2.

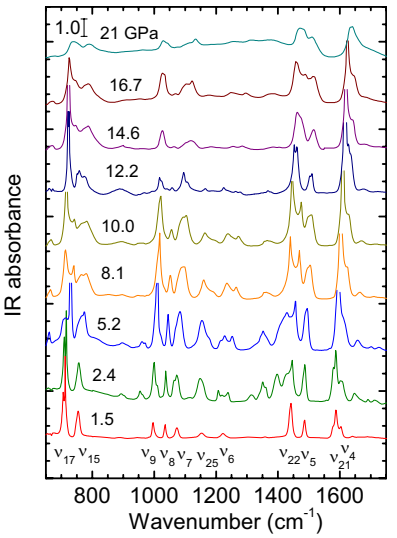

FIG. 5. (Color online) Representative IR spectra of pyridine upon compression in the spectral region of 650–1750 cm^{-1}. Some intense IR absorption bands (e.g., at ~700 and ~1600 cm^{-1}) display a truncated intensity (disconnected line) at the detector saturation level. The absolute absorbance intensity is labeled by the vertical bar at the top left corner. The pressures are labeled above each spectrum. The spectra are offset vertically for clarity.

agreement with their study as shown in Table I. Therefore we conclude that the phase we observed at 1–2 GPa (labeled as II) is consistent with the glassy phase proposed by Heyns and Venter. However, the clearly resolved lattice modes as well as narrow internal modes in both Raman and IR measurements suggest that such glassy phase is crystalline in nature.

It is of fundamental interest to understand the crystal and molecular structures of all the pressure-induced new solid phases. However, there are no *in situ* high-pressure x-ray diffraction data available for pyridine up to date. Due to the fact that pyridine is isoelectronic to benzene and thus exhibits many similarities in molecular structures and properties to benzene, examining high-pressure behaviors of benzene in parallel with pyridine may provide insight into the structures of pyridine in different phases and the nature of the transformations. Indeed, both benzene and pyridine crystallize into an orthorhombic structure at ambient pressure and low temperature although the detailed space groups are different.[16,25,31] At room temperature upon compression to 0.07 GPa, benzene crystallizes into the same space group (*Pbca*) as the one at low temperature.[32] Therefore, we propose that pyridine transforms from a liquid into an orthorhombic structure with a possible low-temperature space group of $Pna2_1$ by analogy. However, Heyns and Venter suggested $P2_1/m$ as a possible space group for this phase (phase I).[26] Apparently, either space group will predict many more lattice modes than observed, so *in situ* high-pressure x-ray diffraction measurements are needed to elucidate the crystal structure of this phase at 1–2 GPa for pyridine.

Despite the intensive spectroscopic and x-ray diffraction studies for benzene at high pressures and/or high temperatures, different versions of benzene *P-T* phase diagram with inconsistent structures and stabilities of different phases have been reported. For instance, upon subsequent compression, benzene was reported to transform to distinct phases II, III, III′, and IV at 1.4, 4, 11, and 17 GPa sequentially.[28] In contrast, in a temperature annealed experiment using IR spectroscopy and x-ray diffraction, phase II was found to persist

TABLE II. Pressure dependence ($d\nu/dP$) of the Raman lattice modes for different phases.

			$d\nu/dP$ (cm^{-1}/GPa)			
Lattice mode	Raman shift (cm^{-1})	Pressure (GPa)[a]	Phase II (2–8 GPa)	Phase III (8–11 GPa)	Phase IV (11–16 GPa)	Phase V (>16 GPa)
1[b]	91	8.1		6.2	2.7	1.6
2	204	15.5				3.4
3	221	11.3			3.0	5.3
4	130	2.0	13.3	11.1	7.8	5.7
5	165	2.0	16.0	12.2	8.6	5.9

[a]The pressure at which the lattice mode was initially observed.

[b]This mode at pressures region of <2 GPa (i.e., for liquid and solid phase I) has a pressure dependence of 47.7 cm^{-1}/GPa.

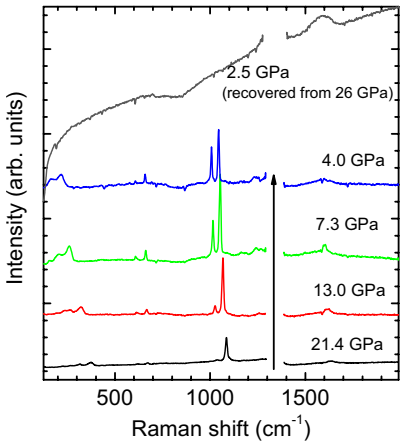

FIG. 6. (Color online) Raman spectra of pyridine upon decompression at selected pressures. The vertical arrow denotes the decompression sequence from the highest pressure of 21.4 GPa. The top spectrum was collected at 2.5 GPa by decompression from 26 GPa.

to above 20 GPa without the observation of phase III or phase III′.[15] Phase II of solid benzene was originally assigned with a monoclinic structure $P2_1/c$,[32] but this structure was later assigned to phase III and only a monoclinic unit cell can be proposed for phase II without detailed space groups.[28] Later x-ray studies on temperature annealed benzene, however, suggest that the monoclinic $P2_1/c$ is associated with phase II which spans the entire pressure region of 1.4–21 GPa. For phase III′ and phase IV structures, similarly, analyses of x-ray diffraction patterns only allow the indexing by monoclinic cell parameters without possible identification of the space groups. Despite the unknown exact high-pressure structures of benzene, we nevertheless note that the phase transition pressures and the number of observed phases of pyridine are reasonably aligned with those for benzene. We therefore propose similar monoclinic structures for pyridine phases II, III, IV, and V analogously. The slight misalignment of the II-to-III phase transition pressures between pyridine and benzene (i.e., 8 GPa vs 4 GPa) suggests that the detailed crystal structures and phase stabilities may differ between the corresponding phases of the two aromatics. The analyses of possible high-pressure structures of pyridine are reported in Table III in comparison with benzene.

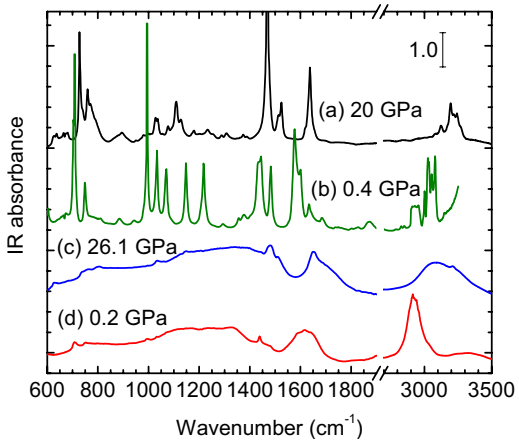

FIG. 7. (Color online) IR spectra of pyridine upon decompression from (a) 20 GPa to (b) 0.4 GPa in comparison with another run with the highest compression pressure of (c) 26.1 GPa and recovered sample at (d) 0.2 GPa. The spectral region of 1900–2700 cm^{-1} was truncated due to the diamond absorption and the lack of characteristic IR modes. The absolute absorbance intensity is labeled by the vertical bar at the top right corner. The spectra are offset vertically for clarity.

TABLE III. Summary of observed high-pressure solid phases of pyridine in comparison with those of benzene.

	Pyridine (C_5H_5N)	Benzene (C_6H_6)
Molecular symmetry	C_{2v}	D_{6h}
Phase	I	I
Pressure range	1–2 GPa	0.07–1.4 GPa
Crystal structure	$Pna2_1$ (C_{2v}^9), $Z=16$ [a]	$Pbca$ (D_{2h}^{15}), $Z=2$ [b]
Phase	II	II
Pressure range	2–8 GPa	1.4–4 GPa
Crystal structure	Monoclinic	Monoclinic[c]
Phase	III	III
Pressure range	8–11 GPa	4–11 GPa
Crystal structure	Monoclinic	$P2_1/c$ (C_{2h}^5), $Z=2$ [c]
Phase	IV	III′
Pressure range	11–16 GPa	11–17 GPa
Crystal structure	Monoclinic	Monoclinic[c,d]
Phase	V	IV
Pressure range	16–22 GPa	17–23 GPa
Crystal structure	Monoclinic	Monoclinic[c,d]
Chemical transformation	>22 GPa	>23 GPa
Structure	Amorphous	Amorphous[d]

[a]Reference 25.
[b]Reference 32.
[c]Reference 28.
[d]Reference 12.

Although no x-ray diffraction data are available, the spectroscopic features such as the increasing number of Raman lattice modes and systematic splittings of several IR internal modes suggest possible transformations from high-symmetry to low-symmetry structures, such as the I-to-II, orthorhombic-to-monoclinic phase transition. Even if the proposed monoclinic phases at higher pressures may actually have similar crystallographic symmetries, to the least extent, we can conclude that there are at least two molecular formulas per unit cell and the compression resulted in significantly enhanced intermolecular interactions within the unit cell. Ciabini *et al.* concluded similarly that high-pressure phases for benzene may have all the same structure with only small deformations of the monoclinic unit cell based on the x-ray

and Raman data.[12] In the case of pyridine, the phase transitions were claimed based on the prominent changes in the lattice phonons but gradual changes in the internal modes, the sluggish behavior of which was also observed in benzene transitions, indicating the high-pressure phases may be metastable.[15] X-ray diffraction and spectroscopic measurements on samples at elevated temperatures may help to understand the high-pressure structures and the nature of phase transitions.

Above 23 GPa, phase changes in benzene were reported to be very gradual with no apparent changes in the C-C bond lengths on compression.[15] A broad peak around 1500–1650 cm^{-1} was observed upon decompression of benzene from above 23 GPa, which was attributed to the CH bending involving sp^3-hybridized carbon atoms. Another broad band around 2900 cm^{-1} indicates the CH stretch from sp^3-hybridized carbon atoms as well. The vibrational frequencies of both of these bands, together with their broad band profiles, can be taken as the evidence of the formation of a cross-linked polymer of high disorder due to a chemical transformation of the initially sp^2 hybridized benzene at this pressure. Both the Raman and IR spectroscopic features of pyridine observed above 22 GPa in this study resembles the high-pressure behavior of benzene above 23 GPa very well. We therefore conclude that pyridine also undergoes such an irreversible chemical transformation via ring opening together with the breaking of the crystal structure, leading to the formation of the amorphous polymerlike substance. Similar irreversible chemical transformations were also observed in thiophene and furan, except that the transformation pressures are lower, i.e., at 16 GPa and 12 GPa, respectively.[3,6] Base on the similar threshold pressure for chemical transformations for benzene and pyridine, i.e., 23 and 22 GPa, it is therefore reasonable to propose that aromatic compounds with similar initial structures may undergo similar pressure-induced transformations.

IV. CONCLUSIONS

Using *in situ* Raman and FTIR spectroscopies, we investigated high-pressure structures and properties of pyridine up to 26 GPa, a pressure far beyond previously achieved. Five reversible phase transitions were observed at around 1, 2, 8, 11, and 16 GPa. These transitions were evidenced by the changes in peak profiles, the number of vibrational modes, as well as the pressure dependence of Raman lattice modes over different pressure ranges. Additionally, an irreversible transformation was identified upon compression to pressures above 22 GPa. This transformation is chemical in nature which can be attributed to the destruction of the pyridine ring and the formation of a cross-linked amorphous material. Possible monoclinic structures are proposed for the observed high-pressure phases of pyridine by comparing the transformation sequence with benzene together with the characterized high-pressure structures of benzene in parallel. These results suggest that aromatic compounds with initially similar structures, such as pyridine and benzene, may behave similarly at high pressures as well.

ACKNOWLEDGMENTS

The authors acknowledge the support from a Discovery Grant and a Research Tools and Instruments Grant from the Natural Sciences and Engineering Research Council of Canada, a Leading Opportunity Fund from the Canadian Foundation for Innovation and an Early Researcher Award from the Ontario Ministry of Research and Innovation. IR measurements were performed at the U2A beamline at the NSLS at BNL. The U2A beamline is supported by COMPRES, the Consortium for Materials Properties Research in Earth Sciences by NSF under Cooperative Agreement No. EAR06-49658, U.S. Department of Energy (DOE), (CDAC), and NSF (DMR).

*Corresponding author. FAX: (519)-661-3022; yang.song@uwo.ca

[1] S. Block, C. E. Weir, and G. J. Piermari, Science **169**, 586 (1970).
[2] P. Pruzan, J. C. Chervin, M. M. Thiery, J. P. Itie, J. M. Besson, J. P. Forgerit, and M. Revault, J. Chem. Phys. **92**, 6910 (1990).
[3] P. Pruzan, J. C. Chervin, and J. P. Forgerit, J. Chem. Phys. **96**, 761 (1992).
[4] L. Ciabini, M. Santoro, R. Bini, and V. Schettino, J. Chem. Phys. **116**, 2928 (2002).
[5] L. Ciabini, M. Santoro, R. Bini, and V. Schettino, Phys. Rev. Lett. **88**, 085505 (2002).
[6] M. Ceppatelli, M. Santoro, R. Bini, and V. Schettino, J. Chem. Phys. **118**, 1499 (2003).
[7] M. Santoro, M. Ceppatelli, R. Bini, and V. Schettino, J. Chem. Phys. **118**, 8321 (2003).
[8] L. Ciabini, M. Santoro, F. A. Gorelli, R. Bini, V. Schettino, and S. Raugei, Nature Mater. **6**, 39 (2007).
[9] M. M. Thiéry and C. Rérat, J. Chem. Phys. **104**, 9079 (1996).
[10] B. P. van Eijck, A. L. Spek, W. T. M. Mooij, and J. Kroon, Acta Crystallogr., Sect. B: Struct. Sci. **54**, 291 (1998).
[11] M. Chandrasekhar, S. Guha, and W. Graupner, Adv. Mater. **13**, 613 (2001).
[12] L. Ciabini, M. Santoro, R. Bini, and V. Schettino, J. Chem. Phys. **115**, 3742 (2001).
[13] K. K. Zhuravlev and M. D. McCluskey, J. Chem. Phys. **114**, 5465 (2001).
[14] K. K. Zhuravlev and M. D. McCluskey, J. Chem. Phys. **117**, 3748 (2002).
[15] L. Ciabini, F. A. Gorelli, M. Santoro, R. Bini, V. Schettino, and M. Mezouar, Phys. Rev. B **72**, 094108 (2005).
[16] A. Budzianowski and A. Katrusiak, Acta Crystallogr., Sect. B: Struct. Sci. **62**, 94 (2006).
[17] C. H. Kline and J. Turkevich, J. Chem. Phys. **12**, 300 (1944).
[18] L. Corrsin, B. J. Fax, and R. C. Lord, J. Chem. Phys. **21**, 1170 (1953).
[19] J. K. Wilmshurst and H. J. Bernstein, Can. J. Chem. **35**, 1183 (1957).
[20] T. D. Klots, Spectrochim. Acta, Part A **54**, 1481 (1998).
[21] J. Turkevich and P. C. Stevenson, J. Chem. Phys. **11**, 328 (1943).
[22] J. Loisel and V Lorenzel, J. Mol. Struct. **1**, 157 (1967).

[23] K. N. Wong and S. D. Colson, J. Mol. Spectrosc. **104**, 129 (1984).
[24] T. Yamamoto, R. Mitsuhashi, M. Akiyama, and Y. Kakiuti, J. Mol. Spectrosc. **117**, 30 (1986).
[25] D. Mootz and H. G. Wussow, J. Chem. Phys. **75**, 1517 (1981).
[26] A. M. Heyns and M. W. Venter, J. Phys. Chem. **89**, 4546 (1985).
[27] A. M. Heyns and M. W. Venter, J. Chem. Phys. **93**, 7581 (1990).
[28] M. M. Thiéry and J. M. Léger, J. Chem. Phys. **89**, 4255 (1988).
[29] H. K. Mao, J. Xu, and P. M. Bell, J. Geophys. Res. **91**, 4673 (1986).
[30] F. P. Ureña, M. F. Gómez, J. J. L. González, and E. M. Torres, Spectrochim. Acta, Part A **59**, 2815 (2003).
[31] J. Akella and G. C. Kennedy, J. Chem. Phys. **55**, 793 (1971).
[32] G. J. Piermarini, A. D. Mighell, C. E. Weir, and S. Block, Science **165**, 1250 (1969).